SUPPORTING INFORMATION

Visible-light-driven photoresponsive color-changing materials with dual light signal outputs and enhanced performance for advanced applications

Ji Fan,[a] Zhaofeng Zheng,[a] Hongqi Li,[a] Zirun Zhan,[a] Wei Wu,[*a] Bolin Ji,[a] Hong Xu,[a] Yi Zhong,[a] Linping Zhang,[a] Zhiping Mao[*abc]

[a] Key Laboratory of Science & Technology of Eco-Textile, Ministry of Education, College of Chemistry and Chemical Engineering, Donghua University, No. 2999 North Renmin Road, Shanghai, 201620, China.

[b] Shanghai Belt and Road Joint Laboratory of Textile Intelligent Manufacturing, Innovation Center for Textile Science and Technology of Donghua University, Shanghai, 201620, China.

[c] National Innovation Center of Advanced Dyeing & Finishing Technology, Shandong Zhongkang Guochuang Research Institute of Advanced Dyeing & Finishing Technology Co., Ltd., Taian City, Shandong Province, 271000, China.

[*] Corresponding authors:

Address: No. 2999 North Renmin Road, Shanghai 201620, China.

Tel: +86-21-67792720; Fax: +86-21-67792707

E-mail address: wuwei@dhu.edu.cn; zhpmao@dhu.edu.cn.

Supplementary Experimental Section

Materials

All chemicals and reagents were used as received without further purification. Cotton fabric (130 g/m^2) was sourced from Saintyear Holding Group Co., Ltd., China. Urea, piperidine, sodium carbonate, 5-chloro-2,3,3-trimethyl-3H-indole, and 5-bromo-2,3,3-trimethyl-3H-indole were obtained from Sinopharm Chemical Reagent Co., Ltd.. 1,4-butanesulfonolactone was provided by Adamas Reagents Co., Ltd.. 5-nitrosalicylaldehyde and salicylaldehyde were purchased from Beijing InnoChem Science & Technology Co., Ltd., while synthetic thickener TF-312E was acquired from Nanjing All-plus Chemical Co., Ltd.. Direct Yellow 27 and Direct Blue 86 from Shanghai Titan Technology Co., Ltd..

Characterization

^{1}H NMR spectra were recorded using a Bruker Avance400 (400 MHz) spectrometer (Germany) with dimethylsulfoxide-d_6 (DMSO-d_6) as the solvent. MS was conducted using a Quadrupole Time of Flight LC/MS system (Bruker impact II, Germany). The chemical structures were characterized by FTIR spectroscopy using a Nicolet iS50 spectrometer (Thermo Fisher Scientific, USA). UV-vis absorption and reflection spectra were measured with a UV-3600 Plus spectrometer (Shimadzu, Japan). Fluorescence spectra were acquired with a FluoroMax-4 spectrophotometer (Horiba Scientific, France). The CIE 1931 color space coordinates were determined using a Datacolor 650 (Datacolor, USA), with the L^* coordinate representing brightness, the a^* coordinate indicating the red-green axis, and the b^* coordinate indicating the yellow-blue axis. TG analysis was conducted using a TG209F1 analyzer (Netzsch, Germany) under a nitrogen atmosphere, covering a temperature range of 30-900 °C at a heating rate of 10 °C/min. All photographs in this study were captured with an iPhone 15. Additionally, a flash lamp (5 W, Ultra fire, 501b, China) with emission wavelengths of 460 nm or 520 nm, as well as a flashlight (5 W, Ultra fire, 501b, China) emitting in the 400-700 nm range, were employed as light sources to assess the photochromic properties of the LCCM and its corresponding solutions.

Density Functional Theory (DFT) calculation

The DFT calculations were performed by the Gaussian16 C.01 software package. In order to find the transition states of the MC before and after photoexcitation, the structure was first geometrically optimized using the B3LYP/6-31+g(d,p) method[1, 2], the D3BJ dispersion correction and the SMD implicit solvent model[3, 4]. Then, the internal reaction path (IRC) is searched based on the transition states to determine the reactants and products in the positive and negative structures. For free energy calculations, the PWPB95/def2-QZVPP method[5, 6], the D3BJ dispersion correction and the SMD implicit solvent model as well as the ORCA 5.0.2 software package[7] were used to calculate high-precision single-point energies of reactants, products and transition states in the gas phase. The solvation free energies are calculated by the difference of single point energy with or without SMD implicit solvent model coupled with M05-2X/6-31g(d) method[8]. Finally, the HOMO-LUMO gap was calculated using the B3LYP/6-311+g(d,p) method, the D3BJ dispersion correction and the SMD implicit solvent model. Multiwfn 3.6[9], Shermo 2.3.6 and VMD 1.9.3 software packages[10] were used in the analysis and plotting process.

Synthesis of MC-1.

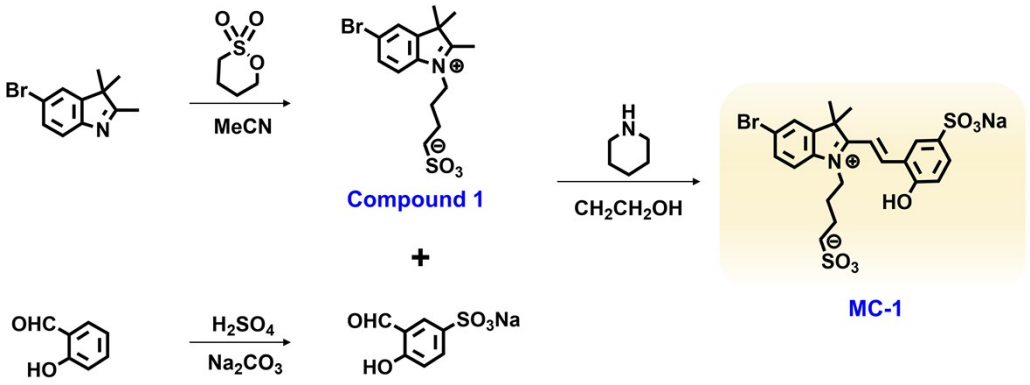

Scheme S1. Synthetic route of MC-1.

3.053 g (25 mmol) of salicylaldehyde was added dropwise to 25 ml of concentrated sulfuric acid in an ice-water bath, and the mixture was reacted at 40 °C for 18 h. After cooling to room temperature, the reaction solution was poured into 150 ml of ice water, and 25 g of solid sodium carbonate was added to neutralize the pH. The precipitate was washed three times with ethanol and acetone, and dried in vacuo

to obtain 3.89 g of 5-sodium sulfonate salicylaldehyde as a white solid product with a yield of about 77%.

5-bromo-2,3,3-trimethyl-3H-indole (10 mmol, 2.38 g) was dissolved in toluene along with three equivalents of 1,4-butanesulfonate. The reaction mixture was heated to 120 °C under a nitrogen atmosphere for 2 hours, after which the reaction was terminated. Following cooling to room temperature, 30 mL of acetone was added, and the solution was stirred overnight at room temperature. The resulting mixture was then subjected to vacuum filtration and washed with acetone three times, yielding compound 1 as a purple-red solid with an 82% yield.

Compound 1 (1 mmol, 0.37 g) and 5-sodium sulfonate salicylaldehyde (1 mmol, 0.22 g) were dissolved in 5 mL of ethanol, followed by the addition of a few drops of piperidine. The reaction mixture was heated to 80 °C for 1 hour. Upon completion of the reaction, the mixture was cooled, allowed to stand, and then subjected to vacuum filtration. The resulting product was dried to yield a bright orange solid with a 79% yield. ^{1}H NMR (400 MHz, DMSO-d_6) δ 11.59 (s, 1H), 8.55 (d, J = 16.3 Hz, 1H), 8.30 (d, J = 2.2 Hz, 1H), 8.20 (d, J = 1.9 Hz, 1H), 7.98 (d, J = 8.7 Hz, 1H), 7.91 (d, J = 16.2 Hz, 1H), 7.82 (dd, J = 8.5, 1.9 Hz, 1H), 7.70 (dd, J = 8.5, 2.1 Hz, 1H), 7.00 (d, J = 8.6 Hz, 1H), 4.58 (t, J = 7.7 Hz, 2H), 2.56-2.49 (m, 4H), 1.98-1.94 (m, 2H), 1.80 (s, 6H).

Synthesis of MC-2.

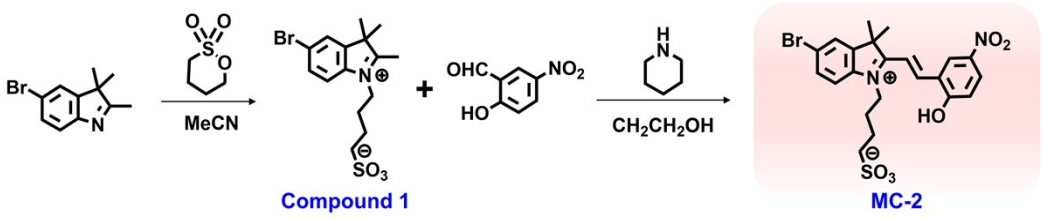

Scheme S2. Synthetic route of MC-2.

Compound 1 (1 mmol, 0.37 g) and 5-nitrosalicylicylaldehyde (1 mmol, 0.17 g) were dissolved in 5 mL of ethanol, followed by the addition of a few drops of piperidine. The reaction mixture was heated to 80 °C for 2 hours. Upon completion, the mixture was cooled, allowed to stand, and then subjected to vacuum filtration. The resulting product was dried to yield a brown-yellow solid with a yield of 45%. ^{1}H

NMR (400 MHz, DMSO-d_6) δ 8.24 (s, 1H), 8.02 (dd, J = 9.1, 2.3 Hz, 1H), 7.33-7.20 (m, 3H), 6.89 (d, J = 8.9 Hz, 1H), 6.61 (d, J = 8.2 Hz, 1H), 6.03 (d, J = 10.3 Hz, 1H), 3.16-3.05 (m, 2H), 2.48-2.35 (m, 2H), 1.98-1.83 (m, 2H), 1.61-1.55 (m, 2H), 1.21 (s, 3H), 1.13 (s, 3H).

Synthesis of MC-3.

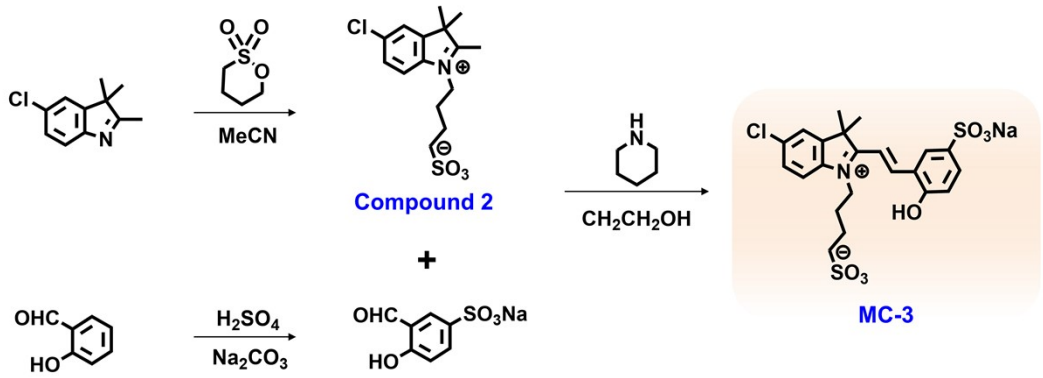

Scheme S3. Synthetic route of MC-3.

5-chloro-2,3,3-trimethyl-3H-indole (3 mmol, 0.58 g) and three equivalents of 1,4-butanesultone were dissolved in toluene and subjected to a reaction at 120 °C for 4 hours under a nitrogen atmosphere. Upon completion, the reaction mixture was allowed to cool to room temperature, yielding a purple-red viscous liquid identified as compound 2, which was subsequently used directly in the next step of the reaction sequence.

Compound 2 (1 mmol, 0.33 g) and 5-sodium sulfonate salicylaldehyde (1 mmol, 0.22 g) were dissolved in 5 mL of ethanol, followed by the addition of a few drops of piperidine. The reaction was carried out at 80 °C for 3.5 hours. Upon completion, the mixture was cooled to room temperature, vacuum filtered, and dried, yielding an orange solid with a 65% yield. ^{1}H NMR (400 MHz, DMSO-d_6) δ 11.58 (s, 1H), 8.54 (d, J = 16.5 Hz, 1H), 8.29 (d, J = 2.1 Hz, 1H), 8.11-8.02 (m, 2H), 7.92 (d, J = 16.4 Hz, 1H), 7.69 (dd, J = 8.4, 2.8 Hz, 2H), 6.99 (d, J = 8.5 Hz, 1H), 4.64-4.52 (t, J = 7.6 Hz, 2H), 2.58-2.51 (m, 4H), 2.02-1.91 (m, 2H), 1.80 (s, 6H).

Synthesis of MC-4.

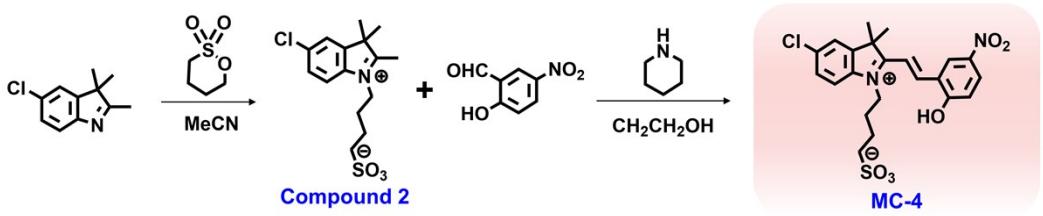

Scheme S4. Synthetic route of MC-4.

Compound 2 (1 mmol, 0.33 g) and 5-nitrosalicylicylaldehyde (1 mmol, 0.17 g) were dissolved in 5 mL of ethanol, followed by the addition of a few drops of piperidine. The reaction was conducted at 80 °C for 1 hour. Upon completion, the mixture was cooled to room temperature, vacuum filtered, and dried, yielding a yellowish-brown solid with a 68% yield. ^{1}H NMR (400 MHz, DMSO-d_6) δ 9.10 (d, J = 2.8 Hz, 1H), 8.50 (d, J = 16.4 Hz, 1H), 8.31 (dd, J = 9.1, 2.8 Hz, 1H), 8.14-7.97 (m, 3H), 7.73 (dd, J = 8.6, 1.7 Hz, 1H), 7.20 (d, J = 9.2 Hz, 1H), 4.64 (t, J = 7.7 Hz, 2H), 3.32-3.28 (m, 2H), 2.01-1.93 (m, 2H), 1.81 (s, 6H), 1.79-1.73 (m, 2H).

Preparation of LCCM.

LCCM was prepared using a screen-printing method, building upon our previous work. Specifically, 0.03 g of the MC compound was precisely weighed and dissolved in 2 mL of water, followed by sonication at 60 °C for 5 minutes to ensure complete dissolution. Subsequently, 0.03 g of urea and 10 g of thickener (1% w.t.) were added to the solution, and the mixture was stirred at 2000 rpm for 30 minutes until achieving full homogeneity. The resulting slurry was then applied to the fabric surface via screen printing, dried at 80 °C for 3 minutes, and stored at room temperature in the dark.

Supplementary Figures

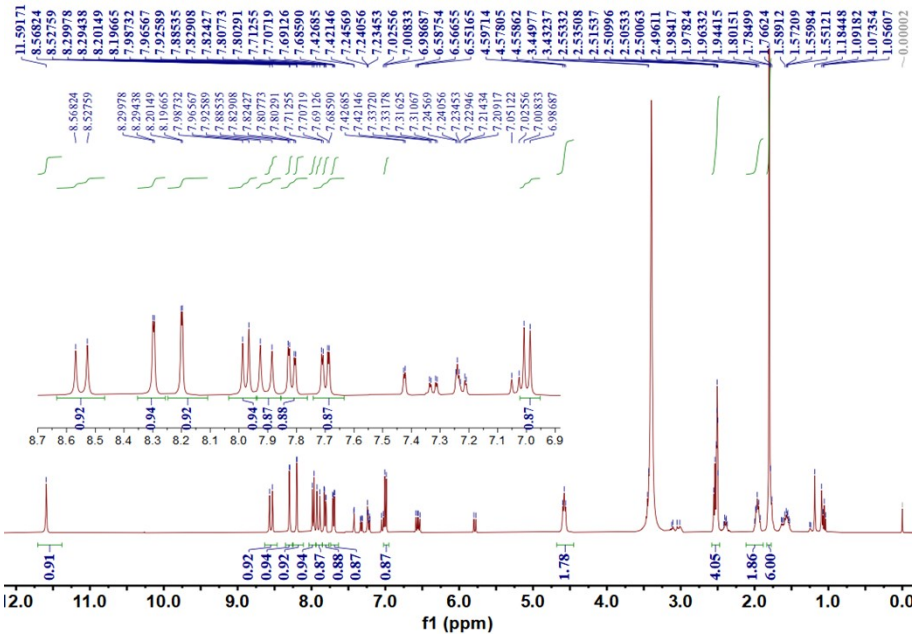

Figure S1. ^{1}H NMR spectra of MC-1. ^{1}H NMR spectra of showed a mixture of the MC-1 and SP-1 coexisted in solution and MC-1 was predominant at room temperature in the dark.

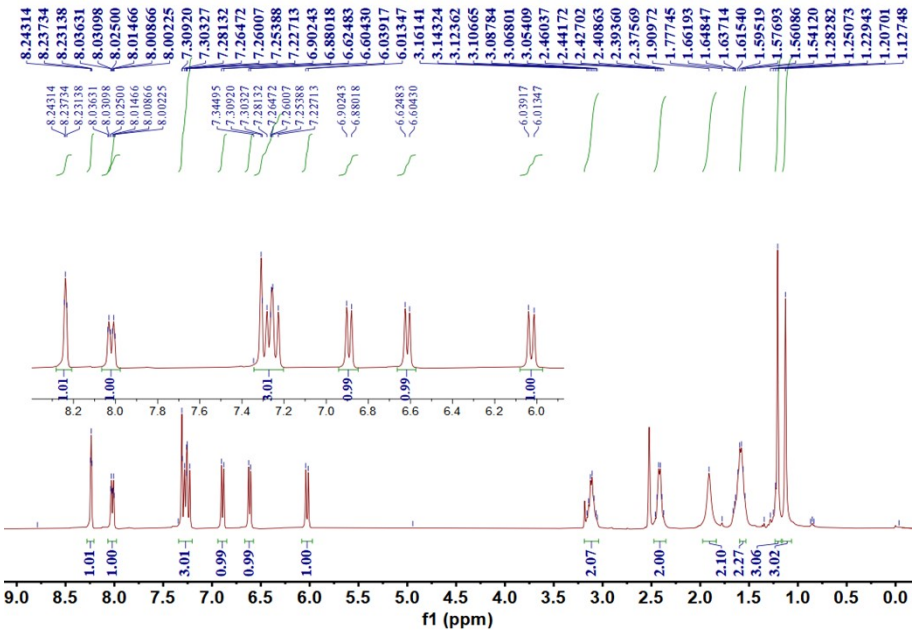

Figure S2. ^{1}H NMR spectra of MC-2. ^{1}H NMR spectra of showed a mixture of the MC-2 and SP-2 coexisted in solution and MC-2 was predominant at room temperature in the dark.

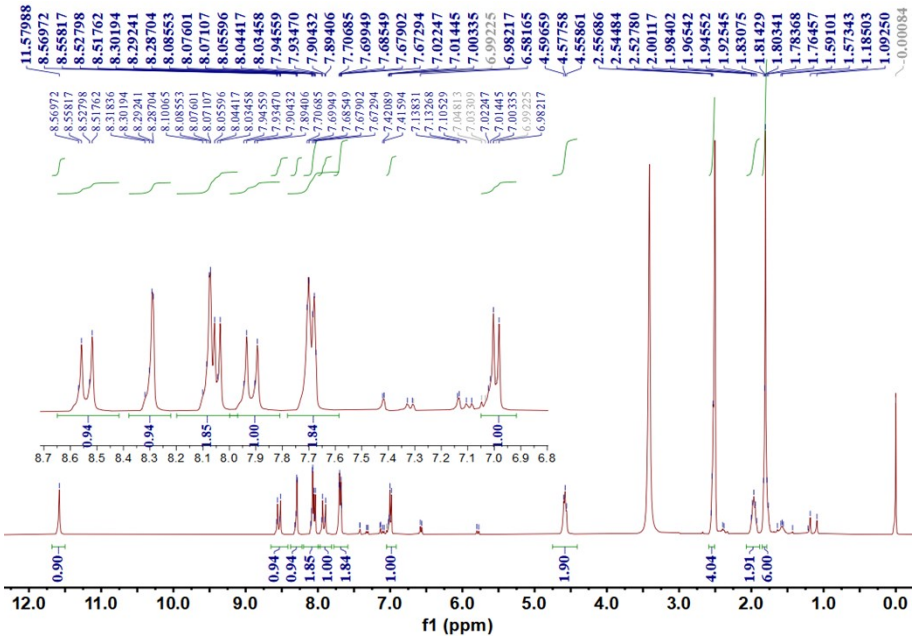

Figure S3. ^{1}H NMR spectra of MC-3. ^{1}H NMR spectra of showed a mixture of the MC-3 and SP-3 coexisted in solution and MC-3 was predominant at room temperature in the dark.

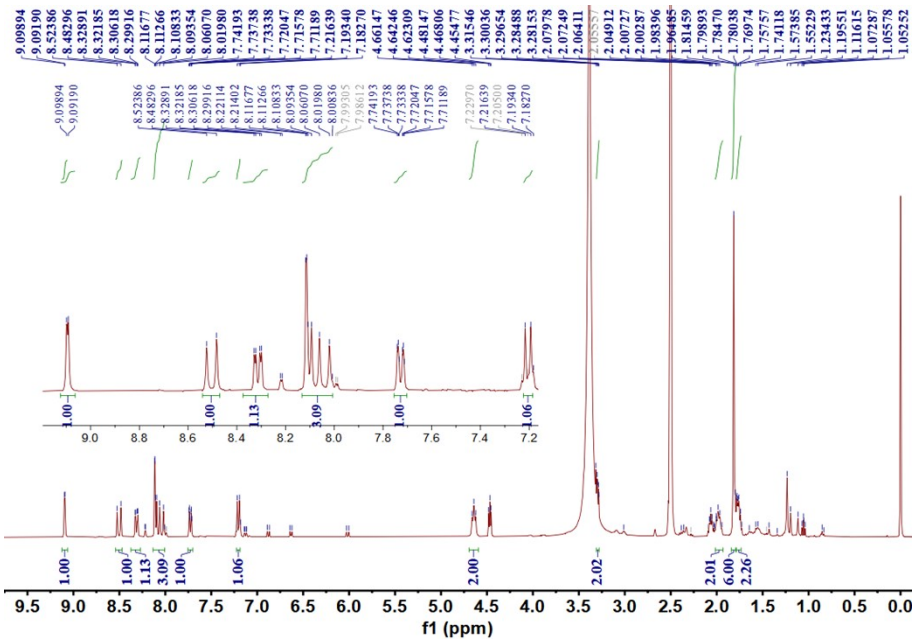

Figure S4. ^{1}H NMR spectra of MC-4. ^{1}H NMR spectra of showed a mixture of the MC-4 and SP-4 coexisted in solution and MC-4 was predominant at room temperature in the dark.

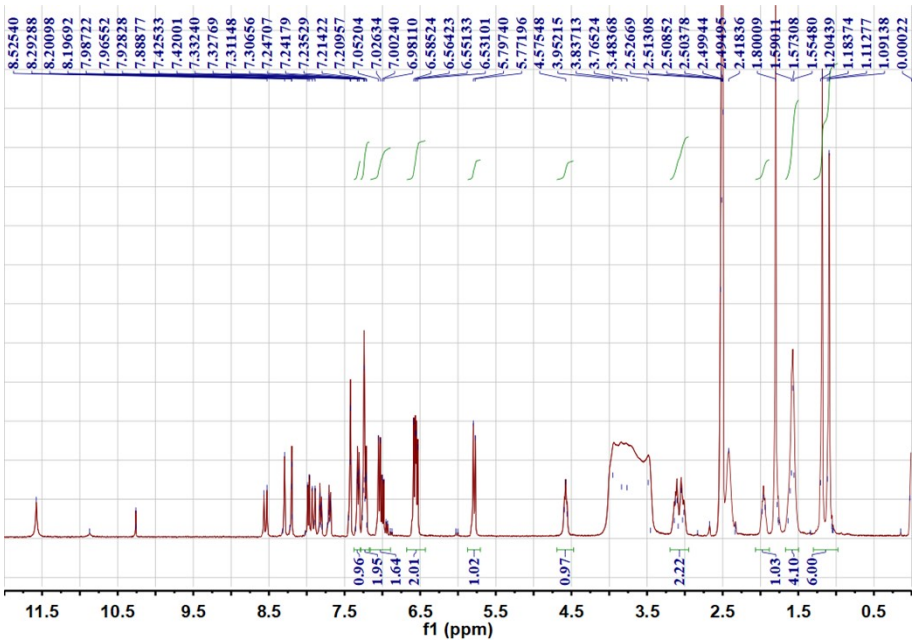

Figure S5. ^{1}H NMR spectra of SP-1. ^{1}H NMR spectra of showed a mixture of the SP-1 and MC-1 coexisted in solution and SP-1 was predominant at room temperature in the daylight.

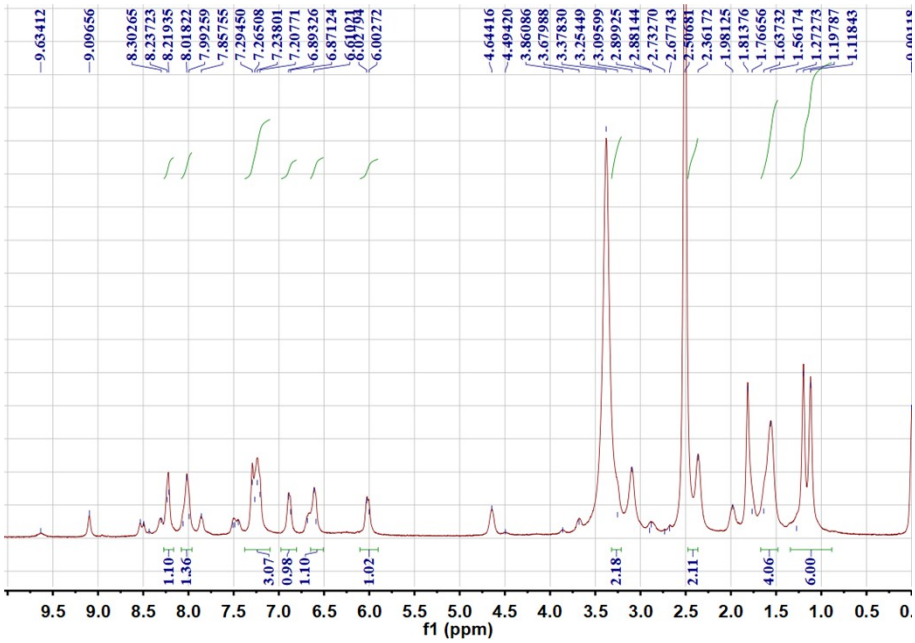

Figure S6. ^{1}H NMR spectra of SP-2. ^{1}H NMR spectra of showed a mixture of the SP-2 and MC-2 coexisted in solution and SP-2 was predominant at room temperature in the daylight.

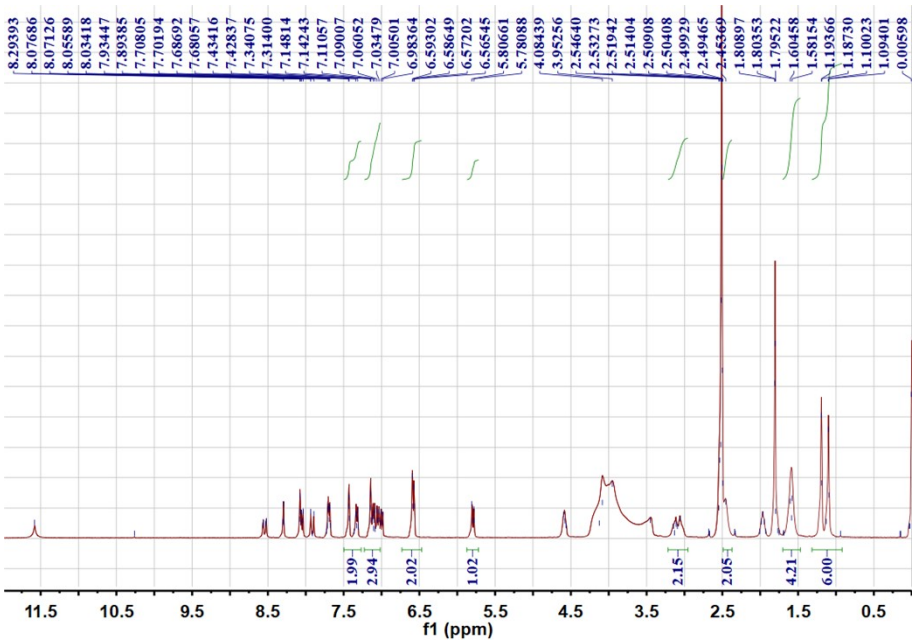

Figure S7. ^{1}H NMR spectra of SP-3. ^{1}H NMR spectra of showed a mixture of the SP-3 and MC-3 coexisted in solution and SP-3 was predominant at room temperature in the daylight.

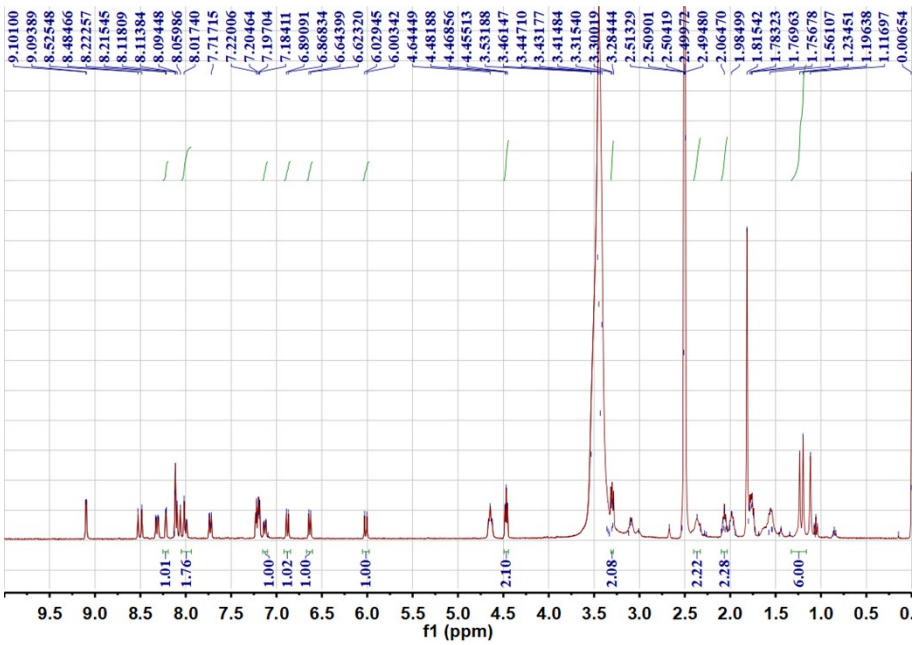

Figure S8. ^{1}H NMR spectra of SP-4. ^{1}H NMR spectra of showed a mixture of the SP-4 and MC-4 coexisted in solution and SP-4 was predominant at room temperature in the daylight.

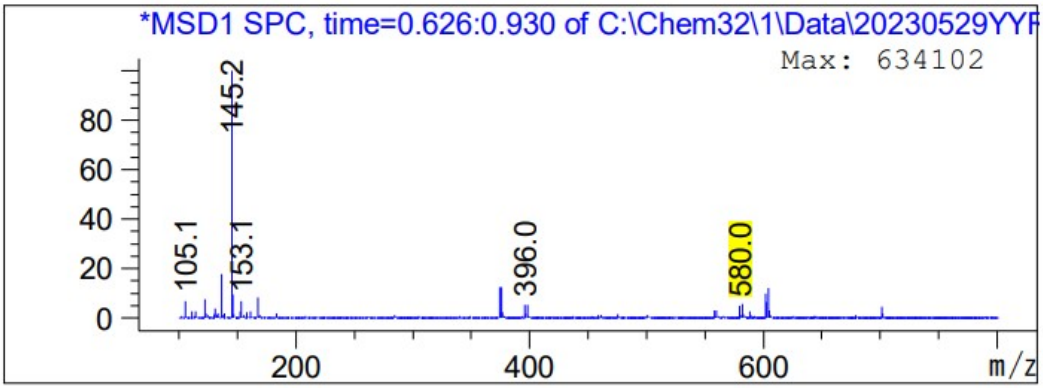

Figure S9. MS spectra of MC-1.

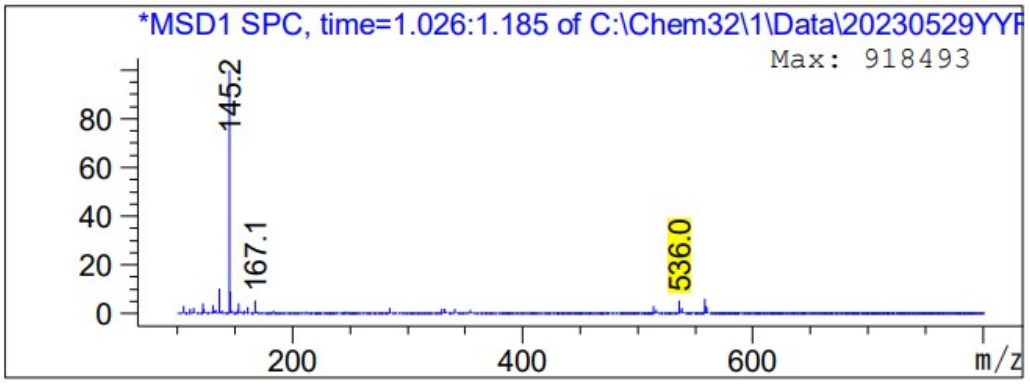

Figure S10. MS spectra of MC-2.

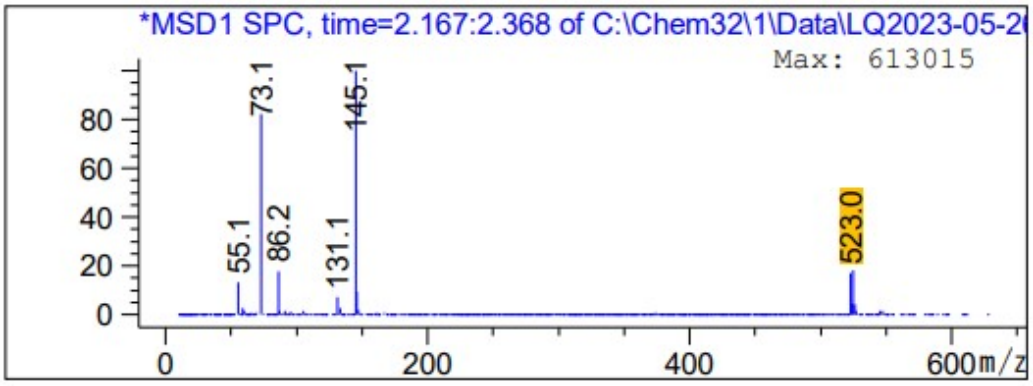

Figure S11. MS spectra of MC-3.

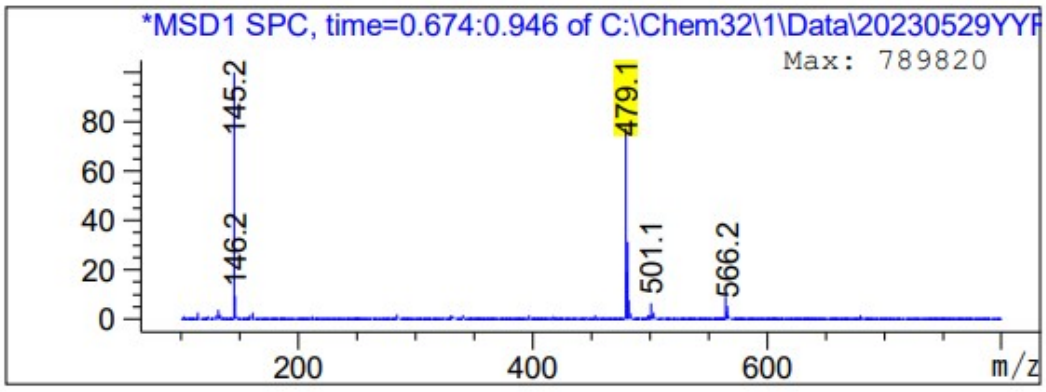

Figure S12. MS spectra of MC-4.

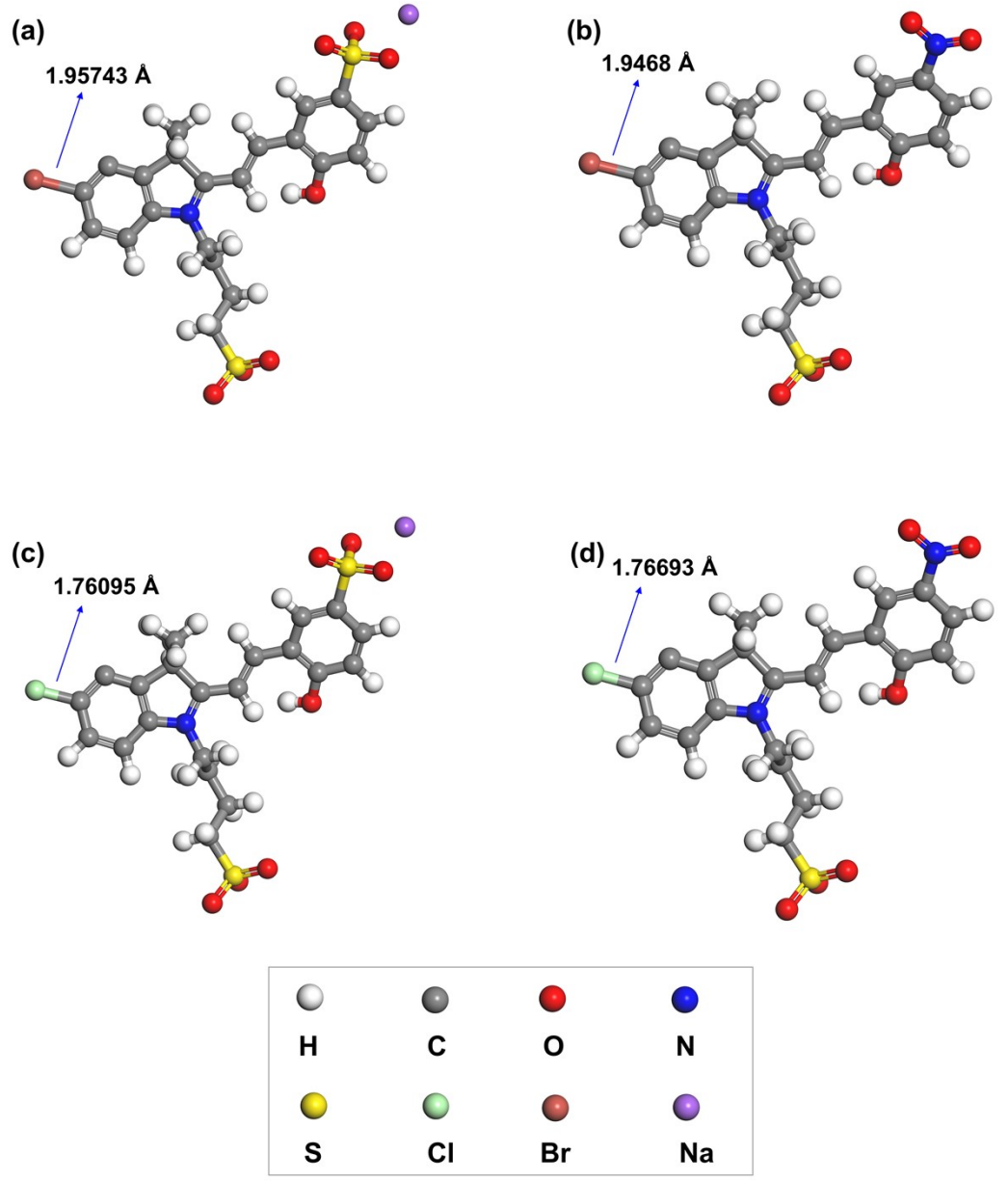

Figure S13. Calculated structures of the four molecules MC-1 to MC-4 and the

corresponding C–Br and C–Cl bond lengths marked nearby.

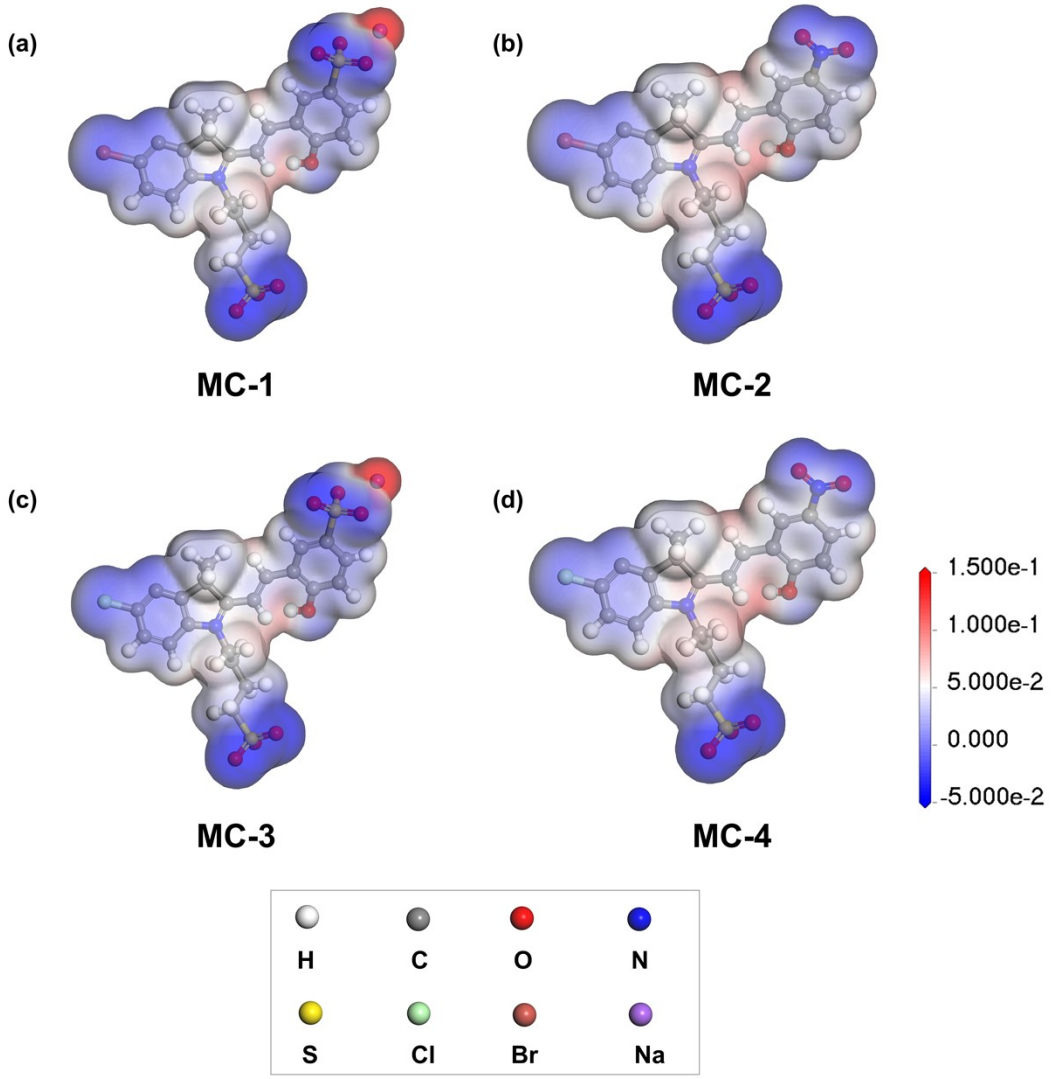

Figure S14. Electrostatic potential distribution of MC-1 to MC-4.

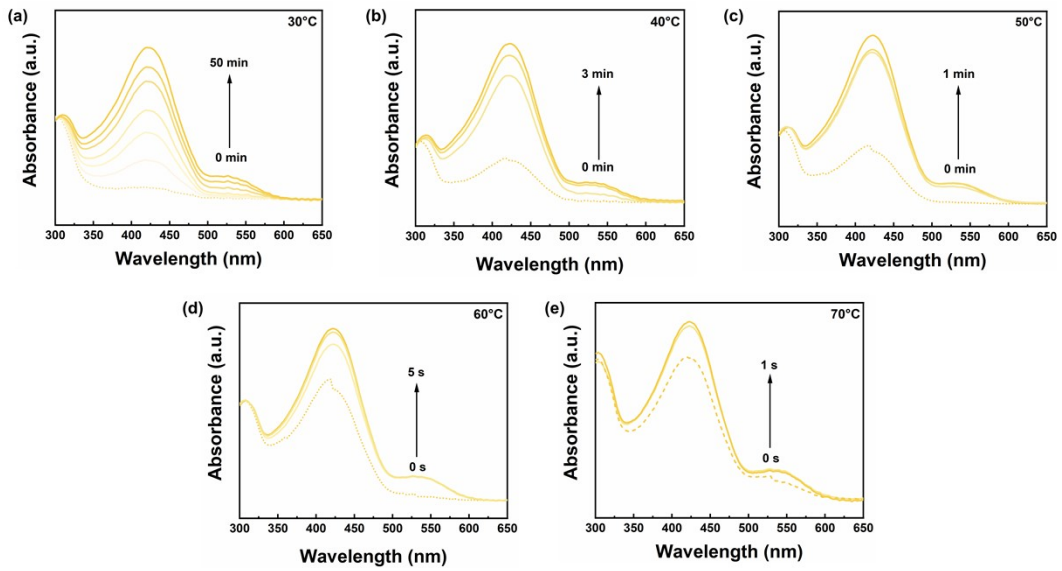

Figure S15. UV-vis absorption of MC-1 (30 μmol/L) in water varies with time after irradiation at different temperatures: (a) 30 °C, (b) 40 °C, (c) 50 °C, (d) 60 °C and (e) 70 °C.

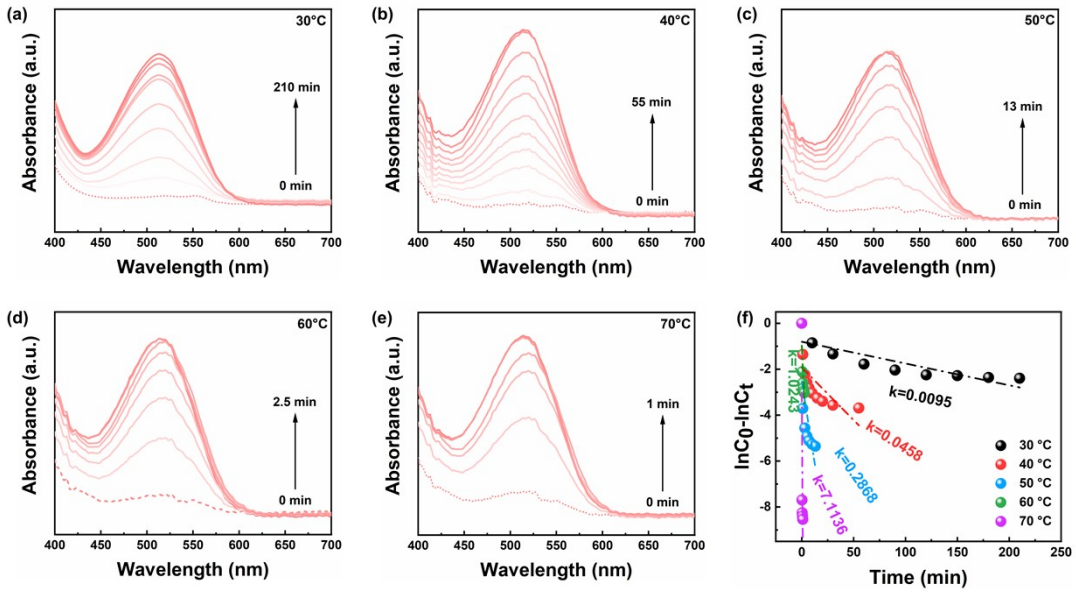

Figure S16. UV-vis absorption of MC-2 (60 μmol/L) in water varies with time after irradiation at different temperatures: (a) 30 °C, (b) 40 °C, (c) 50 °C, (d) 60 °C and (e) 70 °C. (f) Data on the reverse recovery process of MC-2 at varying temperatures, consistent with first-order reaction kinetics. The rate constant (k) is indicated in the figure.

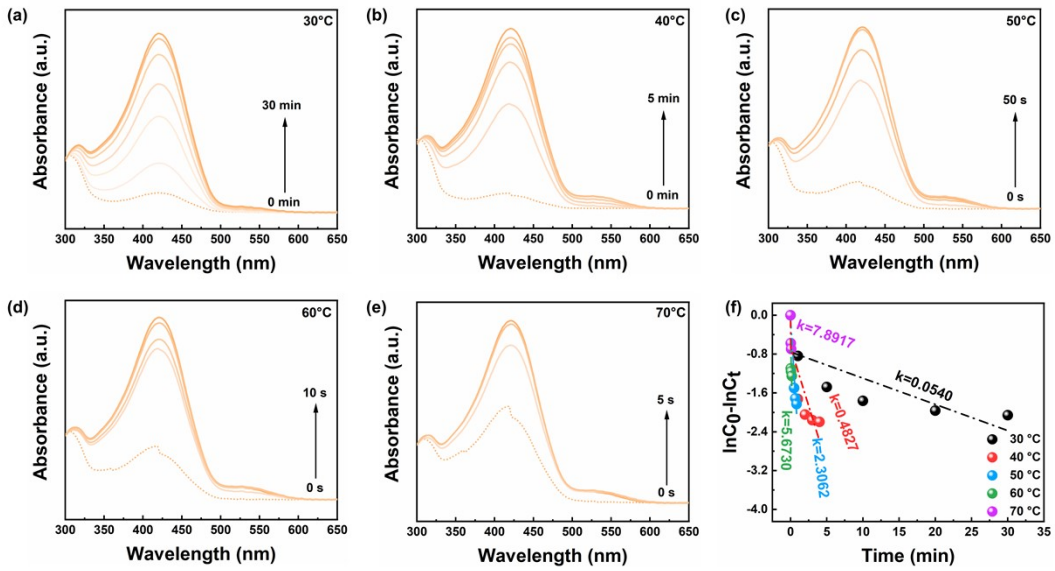

Figure S17. UV-vis absorption of MC-3 (30 μmol/L) in water varies with time after irradiation at different temperatures: (a) 30 °C, (b) 40 °C, (c) 50 °C, (d) 60 °C and (e) 70 °C. (f) Data on the reverse recovery process of MC-3 at varying temperatures, consistent with first-order reaction kinetics. The rate constant (k) is indicated in the figure.

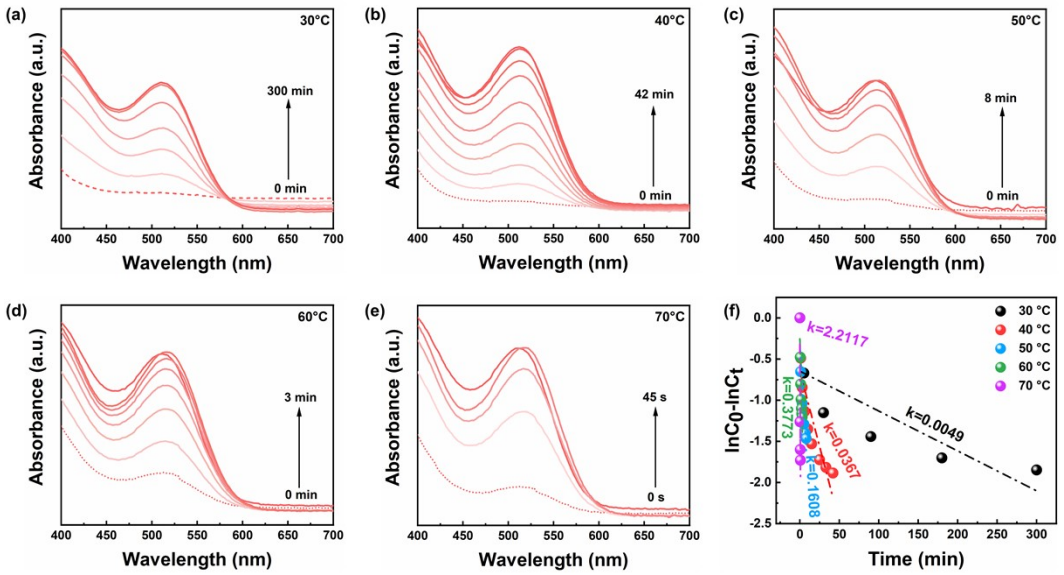

Figure S18. UV-vis absorption of MC-4 (60 μmol/L) in water varies with time after irradiation at different temperatures: (a) 30 °C, (b) 40 °C, (c) 50 °C, (d) 60 °C and (e) 70 °C. (f) Data on the reverse recovery process of MC-4 at varying temperatures, consistent with first-order reaction kinetics. The rate constant (k) is indicated in the figure.

This study investigates the kinetics of the reverse recovery process from MC-1 to MC-4. The process can be approximated by first-order kinetics (Eq. (1)).

$$-dC_t / dt = k\, C_t \qquad (1)$$

Integration of the above equation leads to Eq. (2).

$$\ln C_0 - \ln C_t = -k\, t \qquad (2)$$

Here, C_0 and C_t represent the absorbance in the final color state and the absorbance at illumination time t, respectively. The color recovery process of MC was investigated at five different temperatures (**Figure S15-Figure S18**). The plots of ($\ln C_0 - \ln C_t$), derived from the time-dependent absorbance changes at the maximum absorption peak in the visible region, aligns with the first-order kinetic equation. The rate constant (k) for the recovery process at each temperature was subsequently determined.

Then, according to the Arrhenius equation (Eq. (3)):

$$\ln k = -Ea / RT + \ln A \qquad (3)$$

Where k is the reaction rate constant at temperature *T*; A is the prefactor, also known as the Arrhenius constant; *Ea* represents the apparent activation energy, typically considered temperature-independent; T is the absolute temperature; and R is the molar gas constant. By analyzing the reaction rate constants at various temperatures, a linear relationship between ln k and $1/T$ is established, allowing the apparent activation energy of the MC molecule recovery process to be determined from the slope of the fitted line[11, 12].

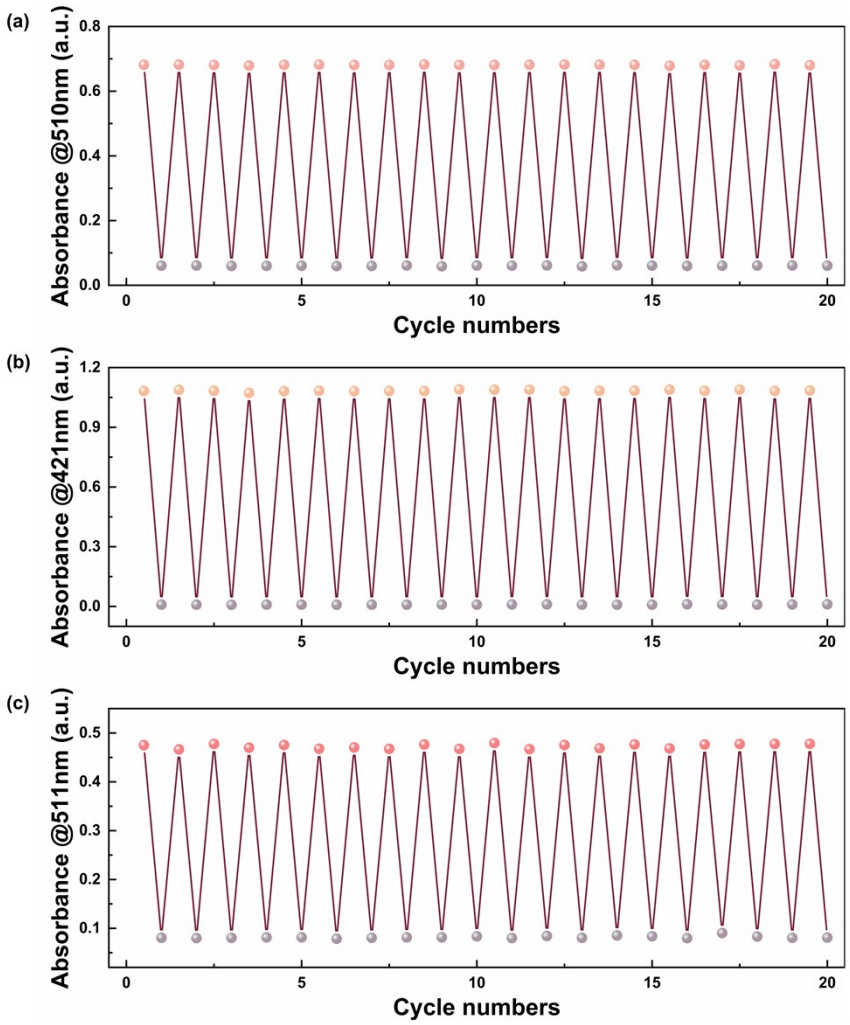

Figure S19. (a-c) Fatigue resistance of MC-2 to MC-4 after 20 alternating cycles, respectively.

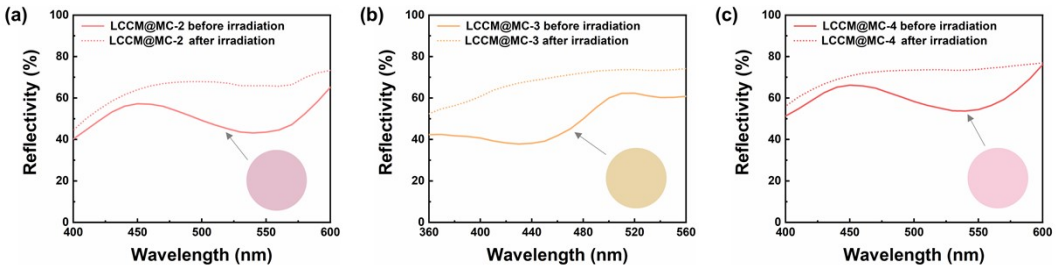

Figure S20. (a-c) UV-vis diffuse reflectance spectra of LCCM@MC-2, LCCM@MC-3 and LCCM@MC-4 before and after irradiation were recorded respectively, and the inset is the corresponding material apparent color picture.

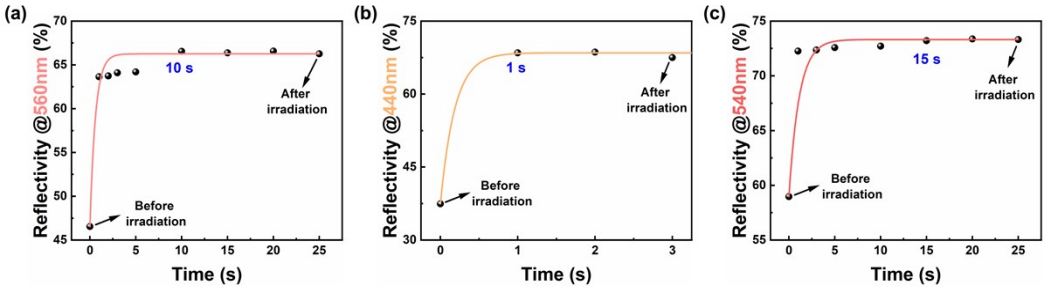

Figure S21. (a-c) The fading rates of LCCM@MC-2, LCCM@MC-3, and LCCM@MC-4 were recorded, respectively.

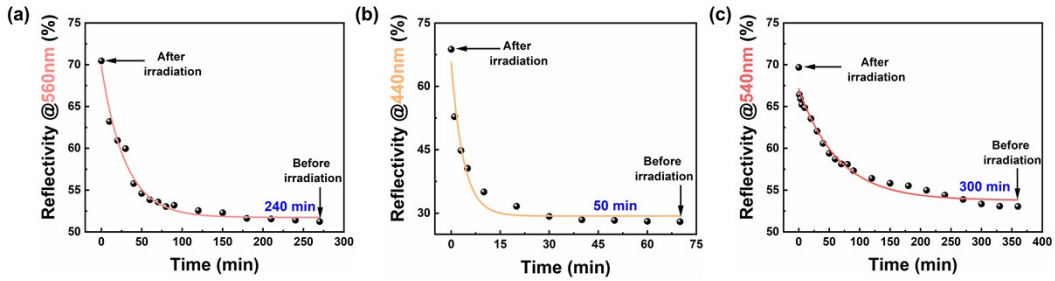

Figure S22. (a-c) The color recovery rates of LCCM@MC-2, LCCM@MC-3, and LCCM@MC-4 were recorded, respectively.

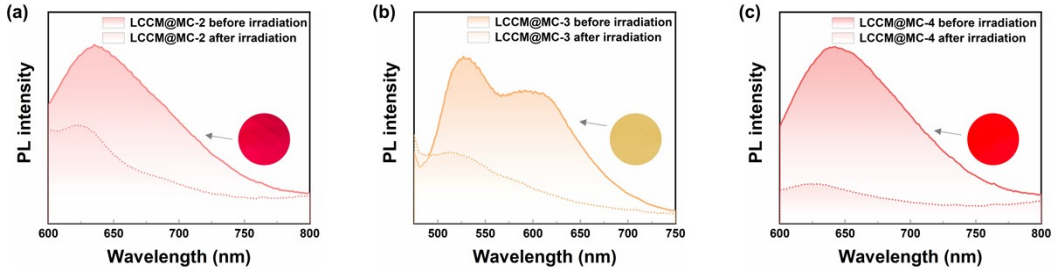

Figure S23. (a-c) Fluorescence spectra of LCCM@MC-2, LCCM@MC-3 and LCCM@MC-4 before and after irradiation were recorded respectively, and the insets are the fluorescence emission images of the corresponding materials.

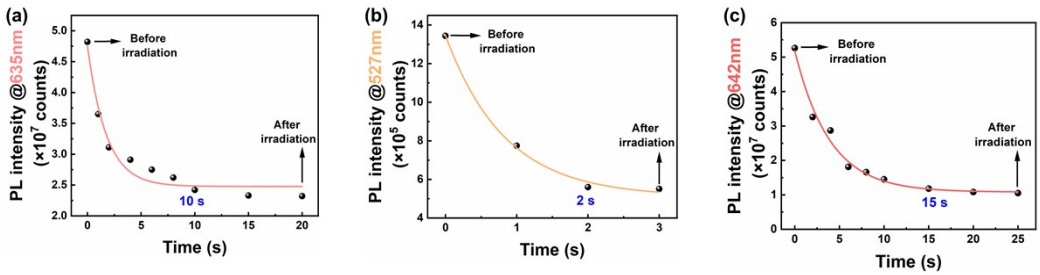

Figure S24. (a-c) Fluorescence quenching rates of LCCM@MC-2, LCCM@MC-3 and LCCM@MC-4 were recorded respectively.

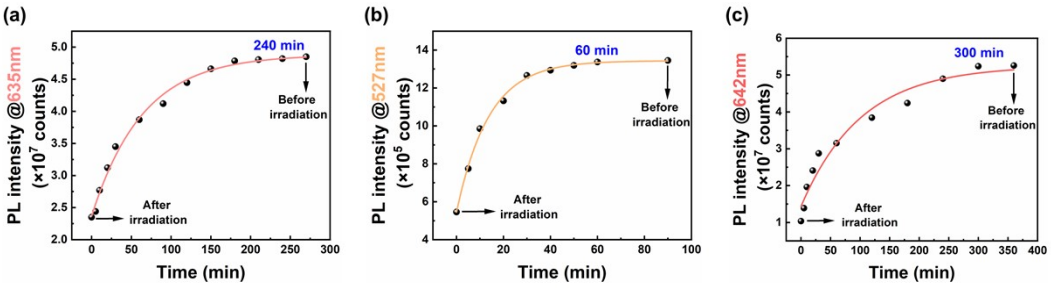

Figure S25. (a-c) Fluorescence recovery rates of LCCM@MC-2, LCCM@MC-3, and LCCM@MC-4 were recorded respectively.

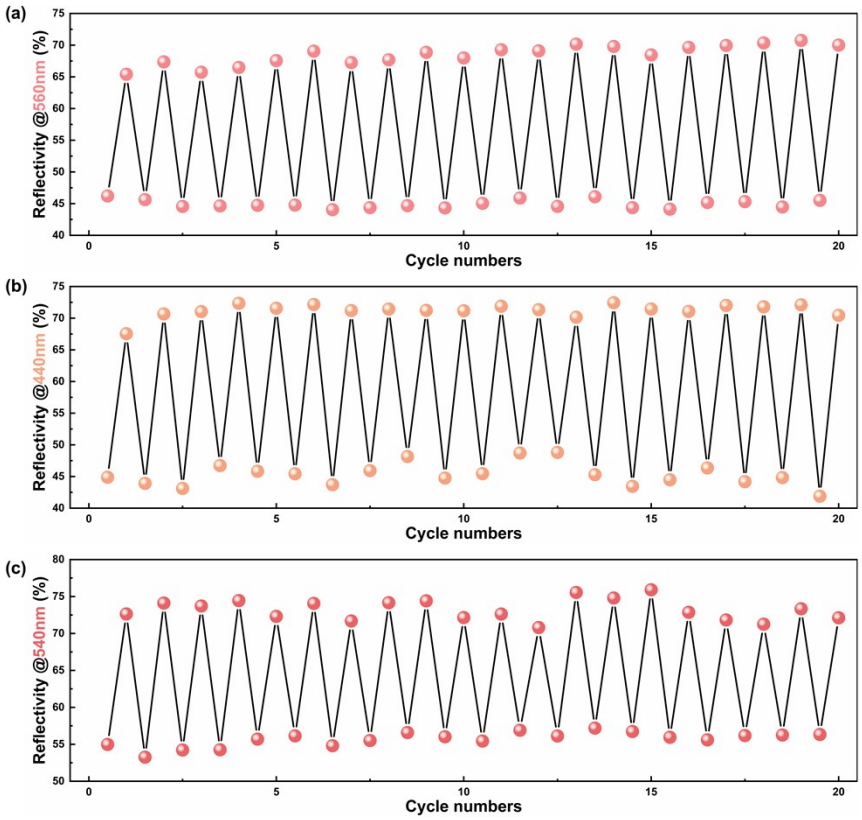

Figure S26. (a-c) Fatigue resistance of LCCM@MC-2, LCCM@MC-3, and LCCM@MC-4 after 20 alternating cycles, respectively.

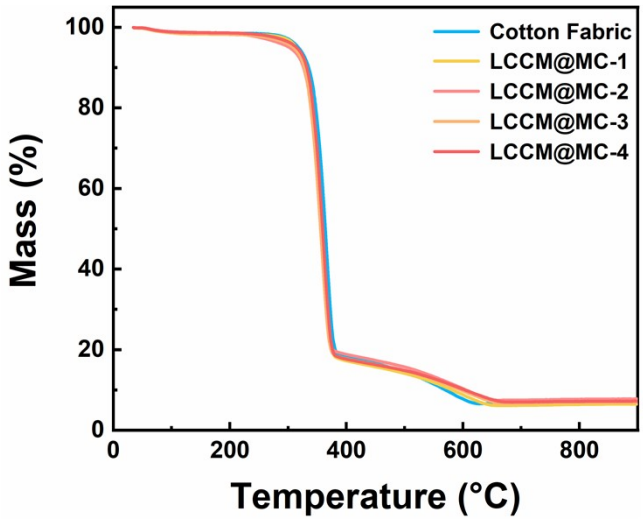

Figure S27. Thermal stability of LCCM.

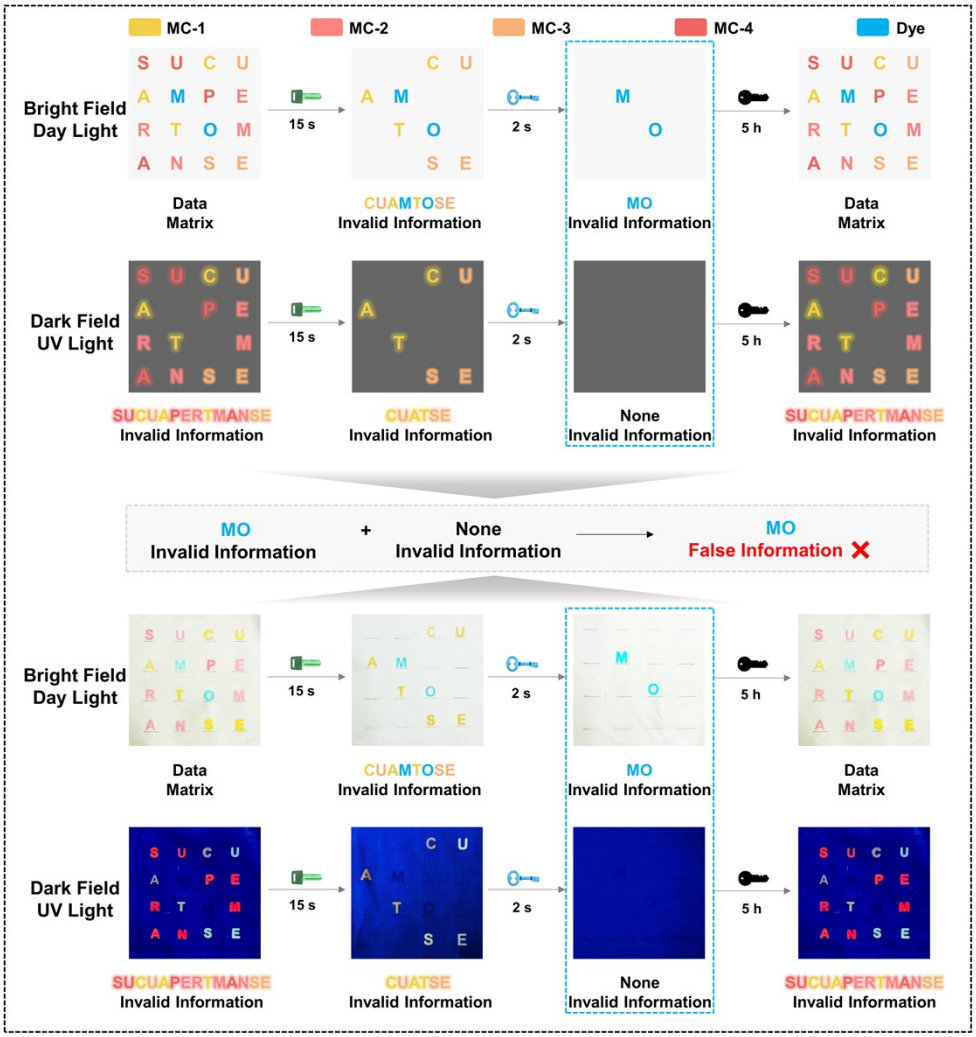

Figure S28. Schematic representation and physical depiction of programmable encryption logic. The applied stimulus sequence involves green light stimulation (520

nm, 15 s), blue light stimulation (460 nm, 2 s), followed by recovery under dark conditions (Dark, 5 h).

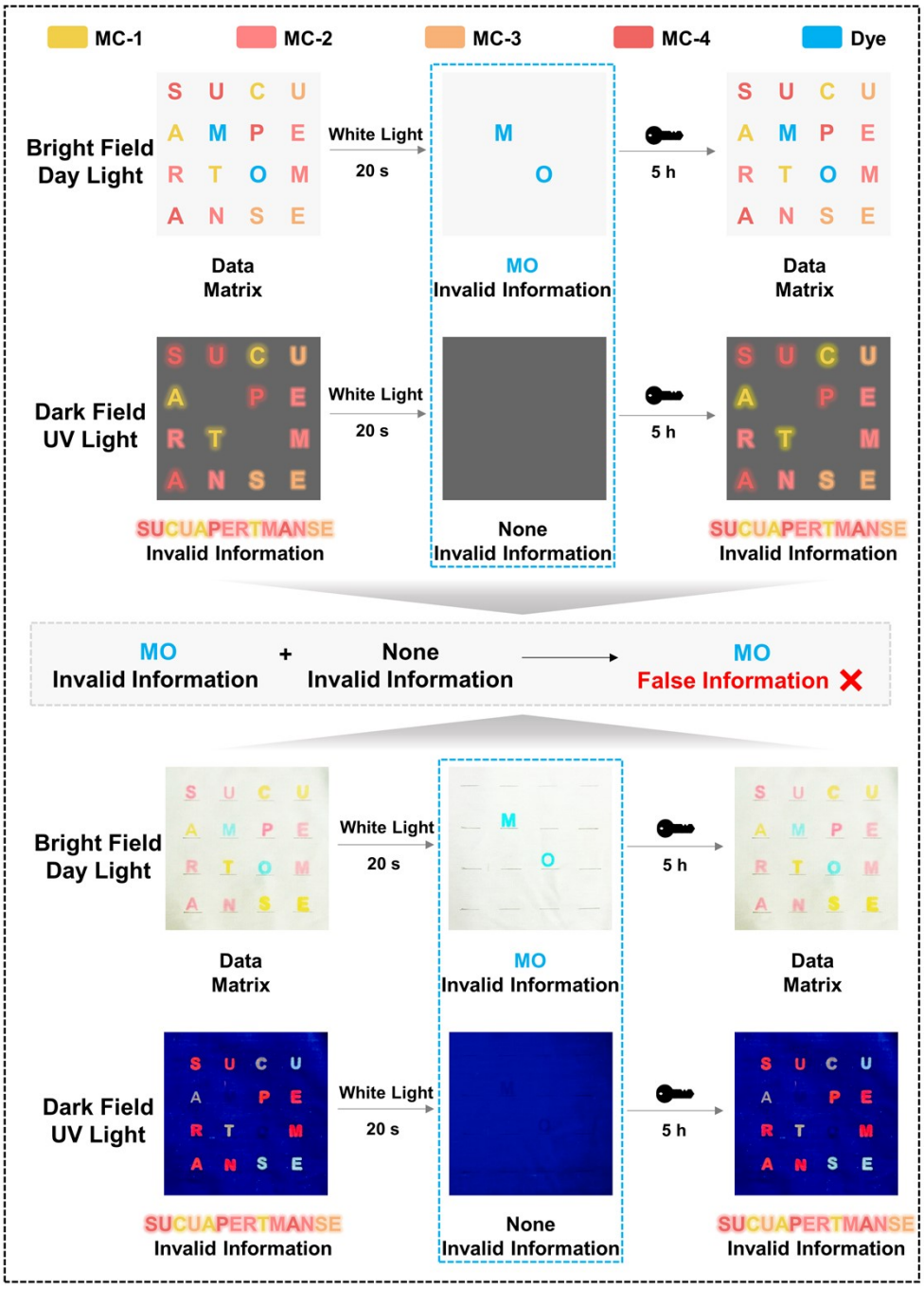

Figure S29. Schematic representation and physical depiction of programmable encryption logic. The applied stimulus sequence includes white light stimulation (400-700 nm, 20 s) followed by recovery under dark conditions (Dark, 5 h).

Supplementary References:

1. F. J. Devlin, P. J. Stephens, J. R. Cheeseman and M. J. Frisch, *J. Phys. Chem. A*, 1997, **101**, 6322-6333.

2. J. R. Hammond, K. Kowalski and W. A. deJong, *J. Chem. Phys.*, 2007, **127**, 144105.

3. S. Grimme, J. Antony, S. Ehrlich and H. Krieg, *J. Chem. Phys.*, 2010, **132**, 154104.

4. A. V. Marenich, C. J. Cramer and D. G. Truhlar, *J. Phys. Chem. B*, 2009, **113**, 6378-6396.

5. L. Goerigk and S. Grimme, *J. Chem. Theory Comput.*, 2011, **7**, 291-309.

6. C. Bannwarth, S. Ehlert and S. Grimme, *J. Chem. Theory Comput.*, 2019, **15**, 1652-1671.

7. B. Shpiro, M. D. Fabian, E. Rabani and R. Baer, *J. Chem. Theory Comput.*, 2022, **18**, 1458-1466.

8. Y. Zhao, N. E. Schultz and D. G. Truhlar, *J. Chem. Theory Comput.*, 2006, **2**, 364-382.

9. T. Lu and F. W. Chen, *J. Comput. Chem.*, 2012, **33**, 580-592.

10. T. Lu and Q. X. Chen, *Comput. Theor. Chem.*, 2021, **1200**, 113249.

11. Z. Du, T. Zhang, H. Gai, L. Sheng, Y. Guan, X. Wang, T. Qin, M. Li, S. Wang, Y.-M. Zhang, H. Nie and S. X.-A. Zhang, *Adv. Sci.*, 2022, **9**, 2103309.

12. J. Fan, W. Wu, Y. Liu, B. Ji, H. Xu, Y. Zhong, L. Zhang and Z. Mao, *ACS Appl. Mater. Interfaces*, 2023, **15**, 54085-54097.